1st International Conference on Multidisciplinary Engagement

Effect of Back Pressure Chamber Size on Scroll Expander Flow Behavior

Habiburrahman[1*], Muhammad Agung Bramantya[2]
[1] *Department of Mechanical and Industrial Engineering, Faculty of Engineering, Universitas Gadjah Mada, Yogyakarta 55281, Indonesia*

Corresponding Author.
**Email*: Habiburrahman.102502@gmail.com

Abstract: *This study investigates the influence of back pressure chamber size on the discharge flow dynamics of a scroll expander in an Organic Rankine Cycle system. The objective is to analyze how variations in chamber volume affect pressure characteristics and flow structures at different crank angles. The methodology involves a comparative analysis of three models with increasing chamber sizes: 260 mm, 300 mm, and 340 mm. The results demonstrate that increasing the back pressure chamber size leads to a consistent reduction in average pressure in both the discharge chamber and outlet. For instance, at a 0° crank angle, the average pressure decreases from 126,175 Pa in Model 1 to 95,466 Pa in Model 3. This pressure reduction is most pronounced during the early discharge phase between 0° and 90° crank angles. However, the relationship with flow stability is non-linear. The intermediate chamber size promotes stronger vortex formation due to higher discharge velocities and localized pressure differences, whereas the largest chamber reduces vortex intensity, thereby improving flow stability. The study concludes that back pressure chamber size is a determining factor in scroll discharge dynamics. Larger chamber configurations effectively reduce pressure levels, although intermediate sizes may induce unfavorable flow instabilities. These findings provide important insights for optimizing expansion devices in waste heat recovery applications.*
Keywords: *Organic Rankine Cycle, Scroll Expander, Back Pressure Chamber, Flow Dynamics, Pressure Distribution*

1. INTRODUCTION

The escalating global energy crisis and the necessity for sustainable development have intensified the focus on low-grade waste heat recovery and renewable energy utilization. Organic Rankine Cycle systems have emerged as a highly effective technology for converting low-temperature thermal energy from industrial processes, solar radiation, and internal combustion engine exhaust into useful mechanical or electrical power [1], [2], [3]. Within these micro-scale ORC units, typically characterized by power outputs below 10 kW, the selection of the expansion device is the most critical factor influencing overall thermodynamic efficiency [4], [5]. Scroll expanders are widely recognized as one of the most promising technologies for such applications due to their high volumetric efficiency, ability to handle liquid-gas mixtures, and simple structure with fewer moving components [6], [7], [8].

Despite their potential, the operational efficiency of scroll expanders is frequently limited by complex internal losses, specifically friction and leakage [9], [10]. Internal leakage consists of radial leakage through axial clearances and tangential leakage through radial gaps, both of which significantly degrade volumetric performance [11], [12]. Research indicates that as clearances increase, leakage mass flow rates rise, whereas excessively tight clearances may lead to mechanical failure due to thermal deformation and friction [4], [9]. To address these challenges, many studies have focused on the modification of scroll geometries, such as the use of variable wall thicknesses, which aim to increase the geometric expansion ratio without enlarging the overall footprint of the machine [13], [14]. For instance, optimizing the compactness factor—the ratio of volume expansion to normalized diameter—has been shown to correlate strongly with isentropic efficiency [15]. The design of efficient scroll machines also requires sophisticated modeling to understand the transient three-dimensional flow field [16], [17]. Computational Fluid Dynamics combined with dynamic mesh technology has become an essential tool for predicting pressure-volume behavior and capturing unsteady suction processes [14], [18]. Such simulations allow

researchers to analyze the non-uniform pressure distributions and vortex formations that occur within the expansion chambers, which are difficult to observe experimentally [13], [17]. Furthermore, semi-empirical and dimensionless models have been developed to characterize performance maps across a wide range of operating conditions, aiding in the preliminary design and sizing of expanders for specific heat sources like solar thermal plants or gasoline engines [5], [7], [19]. Recent advancements have also explored the use of dual-intake-port technology and variable base circle radii to enhance power output and isentropic efficiency [1], [20]. These innovations aim to reduce mechanical losses and improve the pneumatic power conversion efficiency under varying pressure ratios [1], [21]. Experimental validations remain a cornerstone of this field, with various studies testing scroll machines driven by compressed air or specialized refrigerants like R134a [22], [23]. These tests emphasize that while numerical models can predict mass flow rates with high accuracy, factors such as friction coefficients and mechanical efficiency often vary with the pressure ratio and rotational speed [9], [23], [24]. By integrating experimental data with high-fidelity CFD analyses, researchers continue to refine the structural and aerodynamic design of scroll expanders [6], [8].

This study builds upon these foundations by focusing on the numerical analysis of a scroll expander with varying back pressure chamber sizes. By utilizing a structured mesh approach in CFD, we investigate the influence of geometric variations on the internal fluid dynamics. The specific geometric parameters of the scroll profile used in this study are detailed through parametric equations in the methodology section. This research aims to provide a clearer understanding of how housing diameter and back pressure configurations can affect fluid flow behavior specifically at discharge region.

2. METHOD

This research employs numerical simulations to analyze the performance of a scroll expander featuring variations in its back pressure chamber size. The computational analysis was performed using ANSYS FLUENT software to resolve the internal flow characteristics

2.1. Geometry model

The scroll expander geometry is characterized by two identical scrolls. The formation of the scroll geometry is based on several key parameters, including the base circle radius, the initial angles for both inner and outer profiles, and the corresponding ending angles. These parameters define the geometry through equations that serve as the foundation for the expander design [13]. The inner and outer curves of the scroll are defined by parametric equations that calculate coordinates based on the base circle radius and involute angles. These specific geometric parameters are detailed in **Table 1**. Furthermore, the inner and outer involute curves are generated using the mathematical relations presented in **Equation 1, 2, 3, and 4**. Orbiting radius defines the eccentric motion of the scroll expander. This parameter is determined by the previously selected parameters and the clearance between the two scrolls. A clearance of 20 μm is specified between the two scrolls, as it is the maximum value that can capture the expansion of the scroll expander without reducing its performance [25].

Equation for inner involute

$$x_i = a \times \left(\cos(u + \alpha_i) + u \times \frac{\pi}{180} \times \sin(u + \alpha_i)\right) \quad (1)$$

$$y_i = a \times \left(\sin(u + \alpha_i) - u \times \frac{\pi}{180} \times \cos(u + \alpha_i)\right) \quad (2)$$

$$0 \leq u \leq \varphi_i$$

Equation for outer involute

$$x_o = a \times \left(\cos(u + \alpha_o) + u \times \frac{\pi}{180} \times \sin(u + \alpha_o)\right) \quad (3)$$

$$y_o = a \times \left(\sin(u + \alpha_o) - u \times \frac{\pi}{180} \times \cos(u + \alpha_o)\right) \quad (4)$$

$$0 \leq u \leq \varphi_o$$

To investigate the effect of design scale, this study tests three different scroll expander models distinguished by their total diameter. These models consist of diameters of 260 mm, 300 mm, and 340 mm, which are summarized in **Table 2**. The visual representation of these diameter variations is provided in **Figure 1**

2.2. Mesh generation

The discretization of the model was conducted using a structured mesh method. The computational domain is partitioned into three distinct sections: the inlet domain, the rotation or deforming domain, and the outlet

domain. To accurately represent the eccentric motion of the scroll expander, a dynamic mesh technique is implemented, which is controlled via a User Defined Function

Since the dynamic mesh causes continuous deformation during the simulation, specific mesh handling is required to avoid negative cell volume errors. A smoothing method is applied to the dynamic mesh so that the mesh absorbs the scroll's motion while maintaining the total number of elements and the connectivity between them. The specific distribution of elements across the three domains for all three models is presented in **Table 3**, while the visual layout of the structured mesh for each variation is shown in **Figure 2**

Table 1. Parameter of scroll geometry

Parameter	Simbol	Nilai	Unit
Base Circle Radius	a	5.45	mm
Initial Involute Angle (Inner)	α_i	85	°
Initial Outer Involute Angle (Outer)	α_o	5	°
Ending Involute Angle (Inner)	φ_i	1165	°
Ending Involute Angle (Outer)	φ_o	1245	°
Orbiting Radius	R	9.31204	mm
Height	h	50.24	mm

Table 2. Scroll expander diameter variation

Model	Diameter	Unit
1	260	mm
2	300	mm
3	340	mm

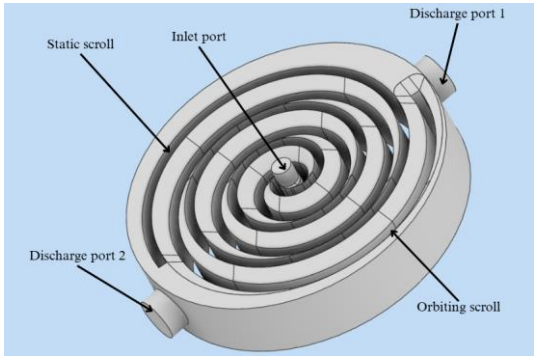

(a)

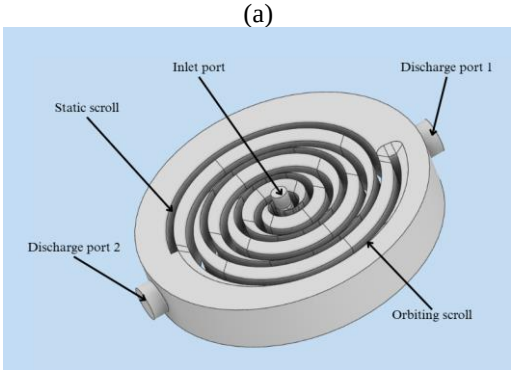

(b)

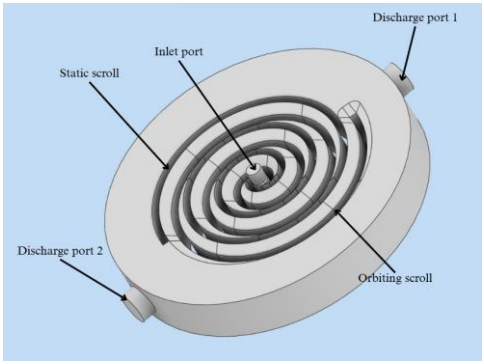

(c)

Figure 1. Variation of scroll expander size: (a) 260 mm, (b) 300 mm, and (c) 340 mm

Table 3. Element number of each model

Domain	Model 1	Model 2	Model 3
Inlet	8680	8680	8680
Deforming	551760	878820	1275315
Outlet	83040	83040	83040

Table 4. Scroll expander operating condition

Parameter	Nilai	Unit
Inlet mass flow rate	0.1937	$\frac{kg}{s}$
Suhu inlet	367	K
Tekanan outlet	176232	Pa
Suhu outlet	320.5	K
Kecepatan putar	1500	rpm

2.3. Boundary condition

The simulation setup incorporates several realistic operating parameters to evaluate performance. The working fluid utilized is R245fa, with its thermophysical properties retrieved from the NIST real gas model library. To synchronize with the rotational frequency of the expander, a transient step size of $1.11e^{-4}$ seconds is used.

The boundary conditions include parameters of fluid at inlet and outlet. Inlet mass flow rate of 0.1937 kg/s at a temperature of 367 K are used for inlet setup. The outlet setup is set to a pressure of 176.232 Pa with a temperature of 320.5 K. The expander operates at a rotational speed of 1500 rpm. Boundary conditions and rotational speed that are used for simulation setup are summarized in **Table 4**

(a)

(b)

(c)

Figure 2. Scroll expander generated mesh: (a) model 1, (b) model 2, and (c) model 3

3. RESULTS AND DISCUSSION

3.1. Pressure Distribution

Figures 3, 4, 5, and 6 illustrate the pressure distribution at crank angles of 0°, 90°, 180°, and 270°. A consistent decrease in average pressure is observed in the discharge chamber and outlet as the size of the back pressure chamber increases. This phenomenon occurs because a larger chamber accommodates a higher volume of gas flow, whereas a smaller chamber leads to fluid accumulation and a subsequent rise in pressure.

This effect is most pronounced during the initial discharge phase between 0° and 90° crank angles. At these angles, the expanded gas begins to exit the chamber. At subsequent angles, most of the fluid has already moved toward the outlet, causing the internal pressure to approach the outlet pressure. Additionally, larger back pressure chambers are associated with higher pressure gradients in the discharge region.

Lower discharge pressure associated with larger chambers may reduce mechanical loading on the scroll components and improve operational reliability. However, excessively low pressure may also reduce the pressure ratio especially at discharge process, potentially decreasing power output. Therefore, the selection of chamber size must balance pressure relief and energy conversion efficiency. Increasing chamber size requires additional material volume and may lead to larger overall system dimensions, which could increase manufacturing cost and limit compactness. This is particularly important in applications such as small-scale waste heat recovery systems, where space and cost constraints are critical.

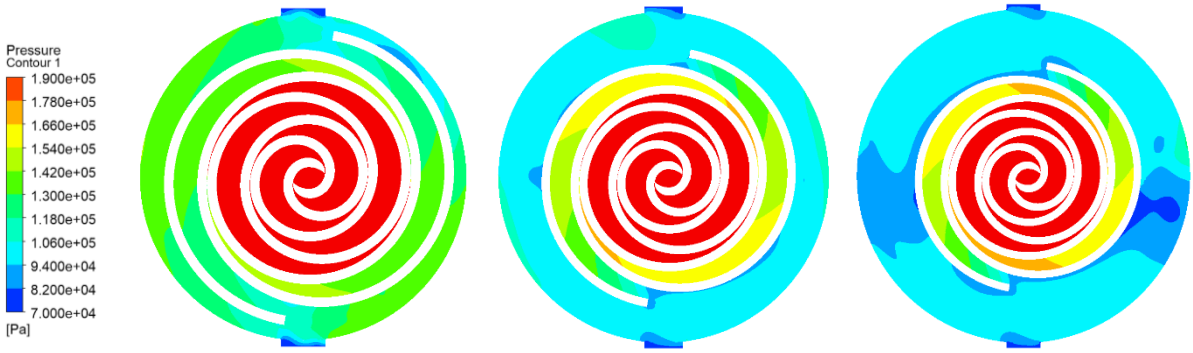

(a) (b) (c)

Figure 3. Pressure distribution at 0°: (a) model 1, (b) model 2, and (c) model 3

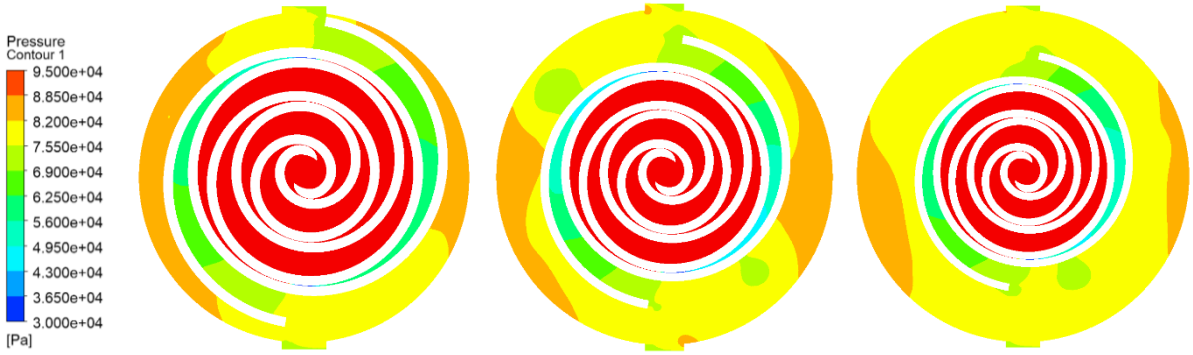

(a) (b) (c)

Figure 4. Pressure distribution at 90°: (a) model 1, (b) model 2, and (c) model 3

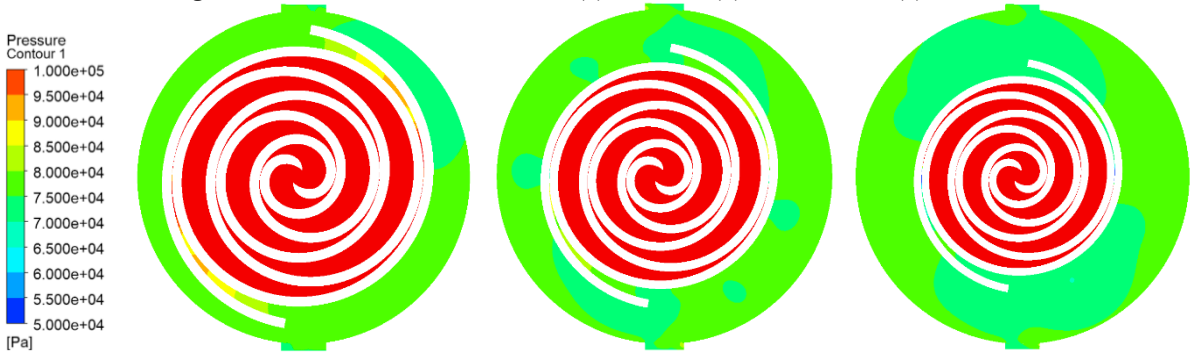

(a) (b) (c)

Figure 5. Pressure distribution at 180°: (a) model 1, (b) model 2, and (c) model 3

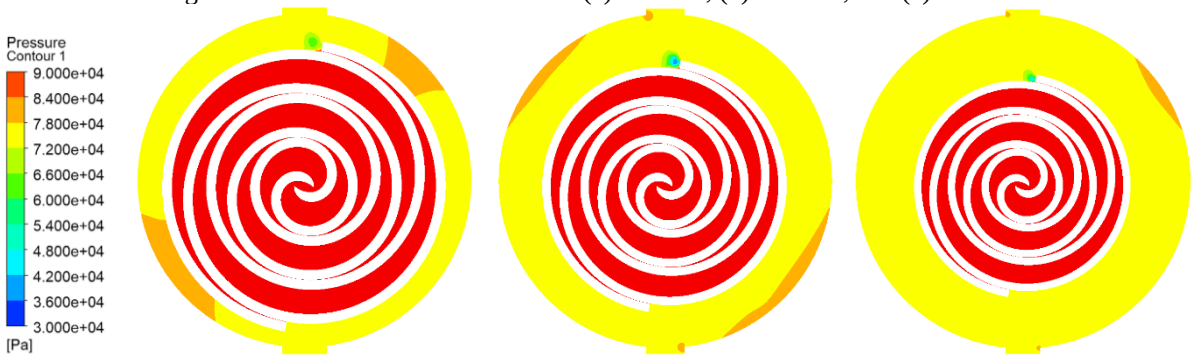

(a) (b) (c)

Figure 6. Pressure distribution at 270°: (a) model 1, (b) model 2, and (c) model 3

Table 5 Average pressure of discharge section

Crank angle	Model 1	Model 2	Model 3
0°	126175 *Pa*	100643 *Pa*	95466 *Pa*
90°	82013 *Pa*	80258 *Pa*	79626 *Pa*
180°	77492 *Pa*	76110 *Pa*	75378 *Pa*
270°	76469 *Pa*	76469 *Pa*	75604 *Pa*

3.2. Streamline and velocity distribution

Velocity profiles were evaluated at the same crank angles (0° to 270°) to identify flow structures. As shown in Figures 7 through 10, the transition from Model 1 to Model 2 increases the occurrence of vortex flow in the discharge area. This is attributed to higher discharge velocities in Model 2 near the static scroll wall, which induce a local pressure drop. The resulting pressure differential draws high-pressure fluid from the back pressure chamber into the discharge area, thereby triggering vortex formation.

Interestingly, further enlargement of the chamber reduces these vortices. This indicates a non-linear relationship between chamber size and flow stability, where intermediate sizes may unintentionally promote turbulence.

Vortex formation increases energy losses, reduce volumetric efficiency, and accelerate wear due to unsteady flow forces. Therefore, designs that operate within this condition may experience reduced performance despite moderate geometric scaling. While larger chambers improve flow stability, they may introduce trade-offs such as increased dead volume, which can negatively impact cycle efficiency. Additionally, larger geometries may complicate manufacturing and integration into compact systems.

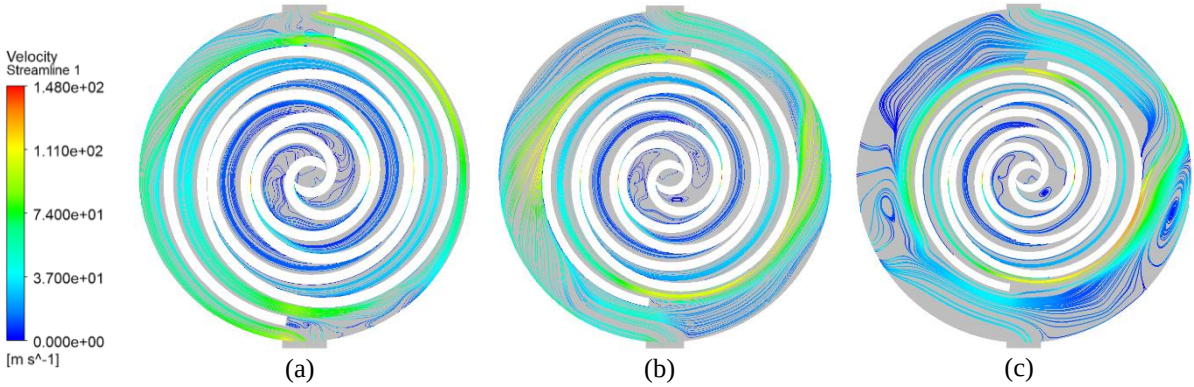

(a) (b) (c)

Figure 7. Velocity distribution and streamline at 0°: (a) model 1, (b) model 2, and (c) model 3

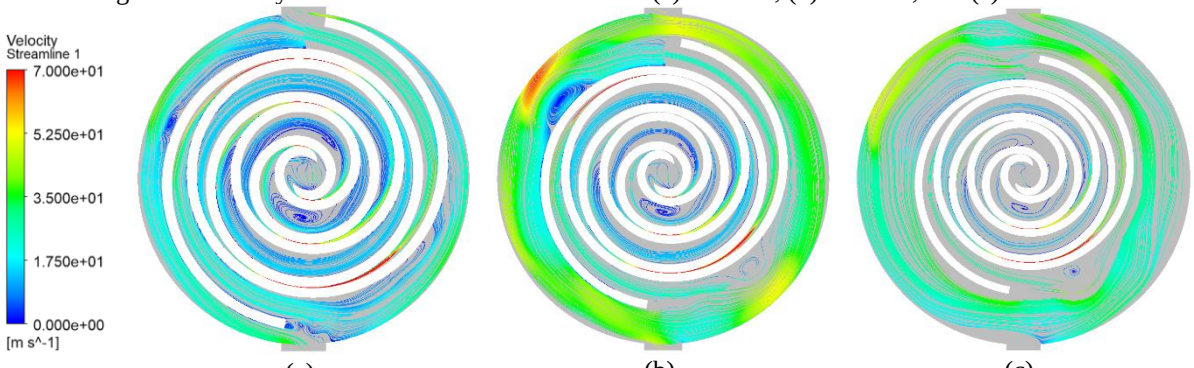

(a) (b) (c)

Figure 8. Velocity distribution and streamline at 90°: (a) model 1, (b) model 2, and (c) model 3

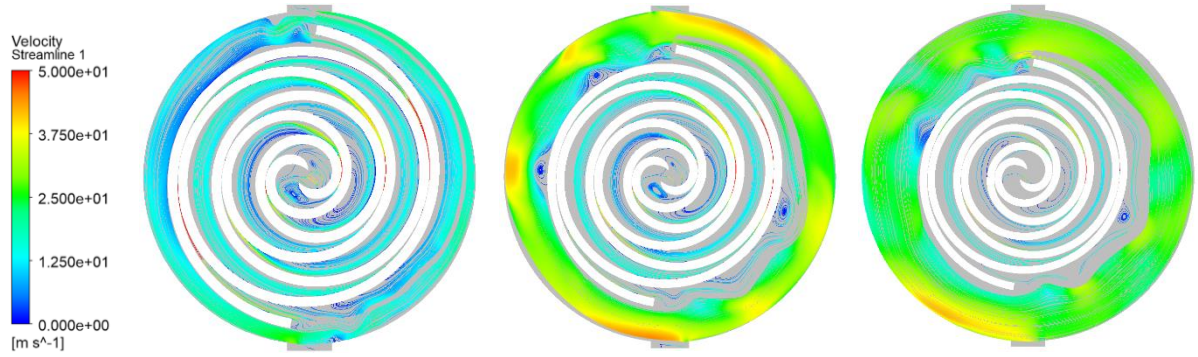

(a) (b) (c)

Figure 9. Velocity distribution and streamline at 180°: (a) model 1, (b) model 2, and (c) model 3

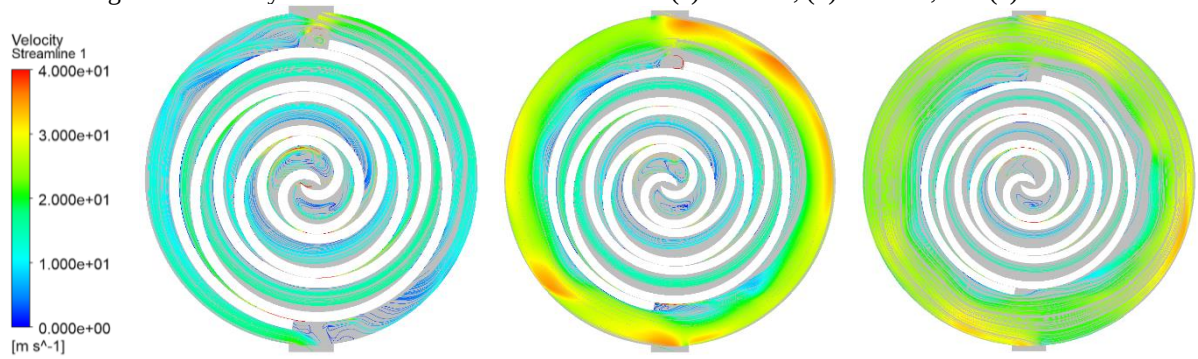

(a) (b) (c)

Figure 10. Velocity distribution and streamline at 270°: (a) model 1, (b) model 2, and (c) model 3

4. CONCLUSION

This study confirms that back pressure chamber size is a determinant factor in scroll discharge flow dynamics.

The size of the back pressure chamber significantly influences the pressure characteristics and flow structures within the discharge region of the scroll expander. An increase in chamber size leads to a consistent reduction in average pressure in both the discharge chamber and outlet due to the larger available volume for gas flow. This effect is most evident during the early discharge phase (0°–90° crank angles), where fluid expansion and outflow begin to dominate the pressure behavior.

In terms of flow structure, variations in chamber size affect the formation of vortices in a non-linear manner. The intermediate chamber size (Model 2) promotes stronger vortex formation due to increased discharge velocity and localized pressure differences near the static scroll wall. However, further enlargement of the chamber reduces vortex intensity, indicating improved flow stability.

Overall, while larger back pressure chambers reduce pressure levels, their impact on flow behavior is more complex, with intermediate configurations potentially inducing unfavorable flow instabilities. These findings highlight the importance of identifying an optimal chamber size that minimizes vortex formation while maintaining efficient pressure utilization.

REFERENCES

[1] F. Fatigati, G. Di Giovine, and R. Cipollone, “Feasibility Assessment of a Dual Intake-Port Scroll Expander Operating in an ORC-Based Power Unit,” *Energies*, vol. 15, no. 3, p. 770, Jan. 2022, doi: 10.3390/en15030770.

[2] T. Saitoh, N. Yamada, and S. Wakashima, “Solar Rankine Cycle System Using Scroll Expander,” *J. Environ. Eng.*, vol. 2, no. 4, pp. 708–719, 2007, doi: 10.1299/jee.2.708.

[3] S. Quoilin, M. Orosz, H. Hemond, and V. Lemort, "Performance and design optimization of a low-cost solar organic Rankine cycle for remote power generation," *Sol. Energy*, vol. 85, no. 5, pp. 955–966, May 2011, doi: 10.1016/j.solener.2011.02.010.
[4] Z. Liu, M. Wei, P. Song, S. Emhardt, G. Tian, and Z. Huang, "The fluid-thermal-solid coupling analysis of a scroll expander used in an ORC waste heat recovery system," *Appl. Therm. Eng.*, vol. 138, pp. 72–82, Jun. 2018, doi: 10.1016/j.applthermaleng.2018.04.048.
[5] L. E. Olmedo, V. Mounier, L. C. Mendoza, and J. Schiffmann, "Dimensionless correlations and performance maps of scroll expanders for micro-scale Organic Rankine Cycles," *Energy*, vol. 156, pp. 520–533, Aug. 2018, doi: 10.1016/j.energy.2018.05.001.
[6] G. Cavazzini, F. Giacomel, A. Benato, F. Nascimben, and G. Ardizzon, "Analysis of the Inner Fluid-Dynamics of Scroll Compressors and Comparison between CFD Numerical and Modelling Approaches," *Energies*, vol. 14, no. 4, p. 1158, Feb. 2021, doi: 10.3390/en14041158.
[7] A. BouguiLa and R. SaiD, "OPTIMIZATION OF A SMALL SCALE CONCENTRATED SOLAR POWER PLANT USING RANKINE CYCLE," *J. Therm. Eng.*, vol. 6, no. 3, pp. 268–281, Apr. 2020, doi: 10.18186/thermal.711287.
[8] M. Morini, C. Pavan, M. Pinelli, E. Romito, and A. Suman, "Analysis of a scroll machine for micro ORC applications by means of a RE/CFD methodology," *Appl. Therm. Eng.*, vol. 80, pp. 132–140, Apr. 2015, doi: 10.1016/j.applthermaleng.2015.01.039.
[9] C. Kutlu *et al.*, "Evaluate the validity of the empirical correlations of clearance and friction coefficients to improve a scroll expander semi-empirical model," *Energy*, vol. 202, p. 117723, Jul. 2020, doi: 10.1016/j.energy.2020.117723.
[10] Y. Lu *et al.*, "Investigation and performance study of a dual-source chemisorption power generation cycle using scroll expander," *Appl. Energy*, vol. 204, pp. 979–993, Oct. 2017, doi: 10.1016/j.apenergy.2017.02.068.
[11] J. Sun, B. Peng, B. Zhu, and Y. Li, "Analysis of Tangential Leakage Flow Characteristics of Oil-Free Scroll Expander for a Micro-Scale Compressed Air Energy Storage System," *Entropy*, vol. 25, no. 2, p. 339, Feb. 2023, doi: 10.3390/e25020339.
[12] J. Wang, "Study On Axial Clearance and Seal of Scroll Compressor," *IOP Conf. Ser. Earth Environ. Sci.*, vol. 267, no. 4, p. 042058, May 2019, doi: 10.1088/1755-1315/267/4/042058.
[13] S. Emhardt, G. Tian, and J. Chew, "A review of scroll expander geometries and their performance," *Appl. Therm. Eng.*, vol. 141, pp. 1020–1034, Aug. 2018, doi: 10.1016/j.applthermaleng.2018.06.045.
[14] S. Emhardt, G. Tian, P. Song, J. Chew, and M. Wei, "CFD modelling of small scale ORC scroll expanders using variable wall thicknesses," *Energy*, vol. 199, p. 117399, May 2020, doi: 10.1016/j.energy.2020.117399.
[15] M. S. Orosz, A. V. Mueller, B. J. Dechesne, and H. F. Hemond, "Geometric Design of Scroll Expanders Optimized for Small Organic Rankine Cycles," *J. Eng. Gas Turbines Power*, vol. 135, no. 4, p. 042303, Apr. 2013, doi: 10.1115/1.4023112.
[16] S. Emhardt, G. Tian, P. Song, J. Chew, and M. Wei, "CFD analysis of the influence of variable wall thickness on the aerodynamic performance of small scale ORC scroll expanders," *Energy*, vol. 244, p. 122586, Apr. 2022, doi: 10.1016/j.energy.2021.122586.
[17] P. P. Song, M. S. Wei, L. Shi, and C. C. Ma, "Numerical simulation of three-dimensional unsteady flow in a scroll expander applied in waste heat recovery," *IOP Conf. Ser. Mater. Sci. Eng.*, vol. 52, no. 4, p. 042017, Dec. 2013, doi: 10.1088/1757-899X/52/4/042017.
[18] E. Fadiga, N. Casari, A. Suman, and M. Pinelli, "Structured Mesh Generation and Numerical Analysis of a Scroll Expander in an Open-Source Environment," *Energies*, vol. 13, no. 3, p. 666, Feb. 2020, doi: 10.3390/en13030666.
[19] A. Legros, L. Guillaume, M. Diny, and V. Lemort, "Modelling, sizing and testing a scroll expander for a waste heat recovery application on a gasoline engine," *IOP Conf. Ser. Mater. Sci. Eng.*, vol. 90, p. 012065, Aug. 2015, doi: 10.1088/1757-899X/90/1/012065.
[20] J. Wei, G. Li, C. Zhang, W. Chang, and J. Wang, "Analysis of Profile and Unsteady Flow Performance of Variable Base Circle Radius Scroll Expander," *Front. Heat Mass Transf.*, vol. 21, no. 1, pp. 199–214, 2023, doi: 10.32604/fhmt.2023.041793.
[21] J. Wei, Q. Hua, L. Yuan, G. Li, J. Wang, and J. Wang, "A review of the research status of scroll expander," *Proc. Inst. Mech. Eng. Part J. Power Energy*, vol. 237, no. 1, pp. 176–197, Feb. 2023, doi: 10.1177/09576509221109245.

[22] P. K. Reddy and M. S. Bhagyashekar, "Experimental testing of scroll machine driven by compressed air for power generation and its integration in small scale organic Rankine cycle," *J. Therm. Eng.*, vol. 7, no. 6, pp. 1457–1467, Sep. 2021, doi: 10.18186/thermal.990826.
[23] Z. Ma, H. Bao, and A. P. Roskilly, "Dynamic modelling and experimental validation of scroll expander for small scale power generation system," *Appl. Energy*, vol. 186, pp. 262–281, Jan. 2017, doi: 10.1016/j.apenergy.2016.08.025.
[24] A. Giuffrida, "Improving the semi-empirical modelling of a single-screw expander for small organic Rankine cycles," *Appl. Energy*, vol. 193, pp. 356–368, May 2017, doi: 10.1016/j.apenergy.2017.02.015.
[25] Y. Du, M. Pekris, and G. Tian, "CFD analysis of flank clearance sizes on micro-scale transcritical CO 2 scroll expander," *Appl. Therm. Eng.*, vol. 232, p. 120980, Sep. 2023, doi: 10.1016/j.applthermaleng.2023.120980.